

# AN AEROMAGNETIC SURVEY OVER THE SHIRASE GLACIER

Kazuo SHIBUYA

*National Institute of Polar Research, 9-10, Kaga  
1-chome, Itabashi-ku, Tokyo 173*

and

Yutaka TANAKA

*Department of Earth Science, Faculty of Science,  
Chiba University, 33, Yayoi 1-chome, Chiba 260*

**Abstract:** The aeromagnetic survey over the Shirase Glacier was for the first time made in 1980 by the 21st Japanese Antarctic Research Expedition. Total force data were acquired in a digital form and reduced to the magnetic anomaly by correcting International Geomagnetic Reference Field and diurnal variations. The obtained anomaly profiles are characterized by low values corresponding to the topographically low area and high values on both sides of the coast in the range from  $-100$  to  $+300$  nT. In order to interpret the obtained anomalies, two-dimensional modeling of subglacial topography was made. The obtained model has a trough of 1800–2000 m depth with 15–20 km width, extending from north to south. The characteristic features of the model topography are consistent with the subglacial topography estimated by the ice-radar and with the sea bottom topography obtained by the echo sounder in the neighboring regions. The magnetic susceptibilities of the rock samples from the eastern regions of the Shirase Glacier were measured in this study. They are mostly in the range of  $10^{-5}$ – $10^{-4}$  emu/cc, though a comparatively larger value of  $1-3 \times 10^{-3}$  emu/cc was obtained for the samples from the southernmost rock areas. The constraints of the ground data on the two-dimensional modeling are discussed.

## 1. Introduction

Aeromagnetic survey is one of the important methods for the studies of large-scale geological structure and subglacial morphology in the antarctic region. It has recently been carried out extensively by many antarctic research expeditions, *e.g.*, RENNER *et al.* (1982) and BEHRENDT *et al.* (1982). As for the Japanese Antarctic Research Expeditions, JARE-8 to JARE-11 and JARE-15 had made a total of 12 flights (2400 miles) using a proton magnetometer on the helicopter or on the aircraft in and around Lützow-Holm Bay. The spatial distribution of the geomagnetic field was summarized as the contour maps of total intensity by TAZIMA *et al.* (1972) or by KANEKO (1976). Since secular variation of geomagnetic field exceeds 100 nT/year, where the notations hereafter are summarized in Table 1, and the diurnal variation is large because of auroral phenomena in the polar region concerned, it is desirable that aeromagnetic surveys be accomplished in a short period by a densely traversed flight. During the wintering of JARE-21, good weather and flight operational conditions enabled us to make 20 flights during October 1980–January 1981, covering Lützow-Holm Bay, the northern part of

Table 1. List of notations.

$D$	Declination of the geomagnetic field, positive for eastward direction. $D$ is negative in the region concerned.
$F$	Total force of the geomagnetic field measured in nT. With the suffix, it means sometimes present field value $F_0$ , time variation $F_{\text{observed}}$ or $F_{\text{diurnal}}$ and regional change $F_{\text{IGRF}}$ or $F_{\text{anomaly}}$ . Ditto for $D$ and $I$ .
$I$	Inclination of the geomagnetic field, positive for downward direction. $I$ is negative in the region concerned.
$i$	Projected dip angle of $I$ onto the $XZ$ plane in Fig. 7. $i$ is negative in the region concerned.
$J$	Magnetization vector with its absolute value $ J $ . $J$ is assumed as homogeneous and parallel to the present geomagnetic field in the region concerned.
$M$	X-component of $J$ in the $XZ$ plane, see eq. (6-3).
$N$	Z-component of $J$ in the $XZ$ plane, see eq. (6-4).
nT	Unit of magnetic flux density of the geomagnetic field, defined as $1 \times 10^{-9}$ Wb/m <sup>2</sup> .
$R, R_1, R_2$	See eq. (6-5) and Fig. 7a.
$S_L, S_R$	See Fig. 7a.
$V(\gamma, \theta, \lambda)$	Geomagnetic potential, see eq. (4). Geomagnetic three components can be mathematically derived from eq. (4).
$X, Y, Z$	Coordinates in the two-dimensional modeling. See Fig. 6 or Fig. 7a.
$X_L, X_R, Z_L, Z_R$	See Fig. 7a.
$\alpha$	$\tan^{-1}\{-(Z_R - Z_L)/(X_R - X_L)\}$ , positive for anti-clockwise direction. $\alpha$ is negative in Fig. 7a.
$\Delta F_{\text{cal}}, \Delta F_X, \Delta F_Z$	Synthetic anomaly in a two-dimensional modeling. See eqs. (5), (6-1) and (6-2).
$\varphi$	Direction of the flight line, measured clockwise from geographic north.
$\kappa$	Magnetic susceptibility. With the suffices E and W, $\kappa_E$ and $\kappa_W$ show model susceptibility to the eastern and western side of the broken curve T-T' in Fig. 6, respectively.
$\Omega$	The angle between $S_L X$ and $X S_R$ , see Fig. 7a.

the Mizuho Plateau, the Shirase Glacier and the Yamato Mountains. The detailed flight log and the obtained magnetic data will be summarized in another report. In this report, we are going to concentrate only on the survey over the Shirase Glacier from the standpoint of working procedures of the interpretation in the antarctic region. The outline of the flight and the data acquisition system is reviewed in the following section. The geomagnetic reference field is given in the third section. The diurnal variation and the synthesized International Geomagnetic Reference Field (IGRF) were reduced from the observed total force data. The reduced geomagnetic anomalies, hereafter referred to as merely the anomalies, are interpreted by a two-dimensionally modeled subglacial morphology on several assumptions. The interpreted subglacial morphology is discussed in relation to the radio-echo sounding and the sea-bottom topography of the neighboring region.

## 2. Survey and Data

The aeromagnetic survey over the Shirase Glacier, hereafter referred to as merely the survey, was made during 1630–1930 LT (1330–1630 UT) on November 27, 1980.

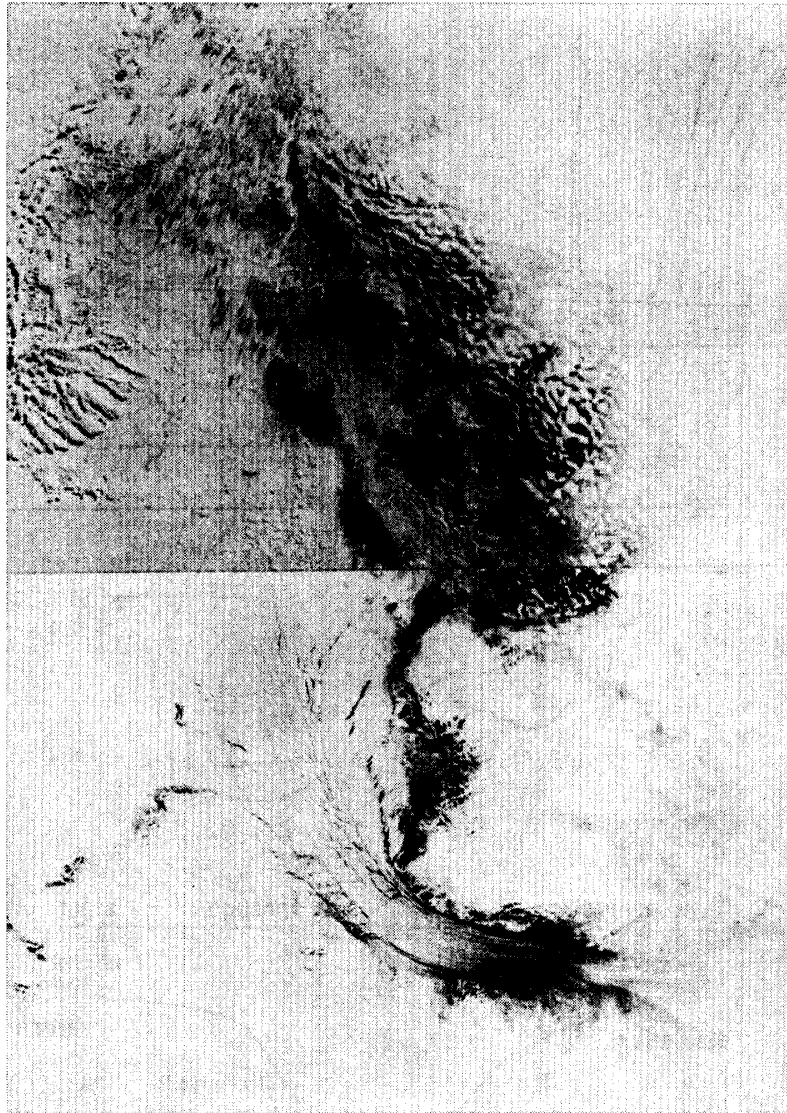


*Fig. 1. LANDSAT image of the Shirase Glacier.*

Against our expectation,  $\omega$ -navigation system was not available because of weak receiving signals and/or non-reliable repeatability of the positioning at the known point, and so the positioning had to be made only visually. Figure 1 illustrates the LANDSAT image of the Shirase Glacier in January 1974. The flight course was so planned that the five flight lines would almost vertically intersect the flow trend, presumably the topographic trend as schematically illustrated by S1-S5 in the upper part of Fig. 2. The flight course was controlled by the magnetic compass on the aircraft, Pilatus-Porter PC-6, in order to keep the flight lines as parallel as possible. The flight speed was controlled at 98 knots against air. The flight height was controlled at 3200 ft above sea level by the barometer and the height above ice was sometimes monitored by the radar altimeter as schematically illustrated in the lower part of Fig. 2. The superposition of the flight line onto the 1:250000 topographic sheet of Lützow-Holm Bay was made by the cross time of the aircraft through each rock area under each flight line.

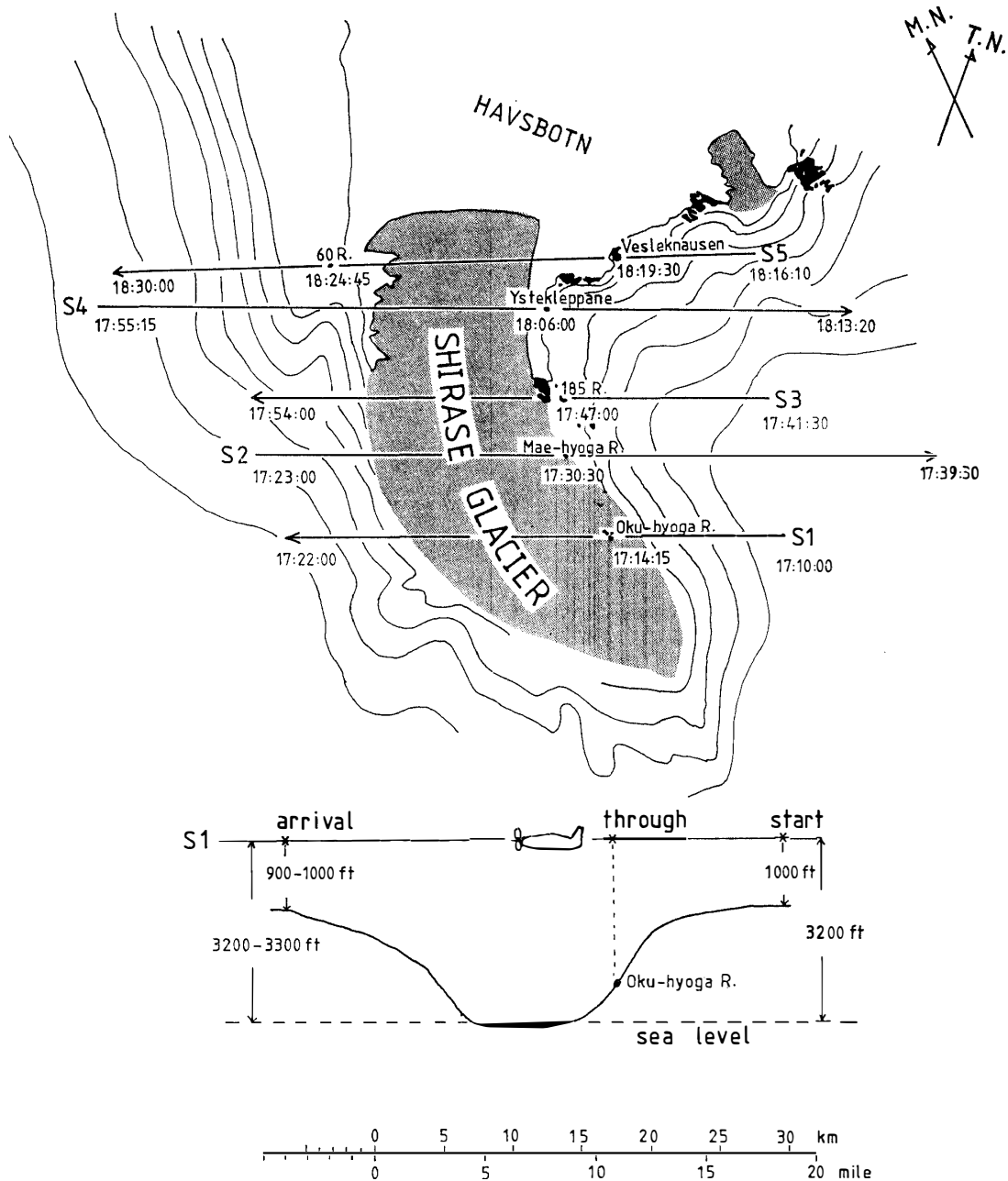


Fig. 2. Schematic flight lines of the aeromagnetic survey over the Shirase Glacier.

Figure 3 illustrates the block diagram of the used proton precession magnetometer (M-123 magnetometer by Barringer Research Ltd.). The earth's geomagnetic field was sensed by the towed head which was cabled by the 10 m-long coaxial cable. The total intensity as a function of Larmor frequency was multiplied in the phase lock loop and was counted for about 0.37 s to give direct count on the 5-digit counter, to be recorded on the analog chart recorder and on the digital cassette tape or the digital printer to the resolution of 1 nT every 1.2 s. The flight speed of 98 knots and the sampling interval of 1.2 s result in a spacial sampling of 60 m/point, approximately.

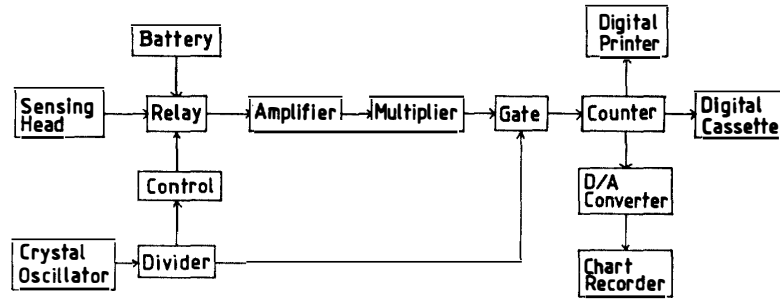


Fig. 3. Block diagram of the proton magnetometer.

### 3. Geomagnetic Reference Field

The geomagnetic secular variation in the antarctic region during 1960–1975 has been examined by NAGATA (1982) from the analysis of geomagnetic three components at 20 stations in the southern hemisphere. The obtained maximum positive annual rate is over 150 nT/year in the vertical component in a polar area of 70°–85°S in latitude and 20°W–60°E in longitude. Figure 4 summarizes the secular variation at Syowa Station (69°00'S, 39°35'E) during 1966–1981 and the open circles in each figure illustrate the observed total force  $F$ , the inclination  $I$  and the declination  $D$ , respectively from the upper to the lower part, where the values are taken from the annual reports of JARE-7 to JARE-22. The above secular variations can be expressed in the quadratic form by a least squares method as follows:

$$F_{\text{secular}} = 46594 - 136.3T + 0.87T^2, \quad (1)$$

(unit : nT)      S.D. = 37.2 nT

$$-I_{\text{secular}} = 65^\circ 54.9' - 4.61'T + 0.04'T^2, \quad (2)$$

S.D. = 2.1'

$$-D_{\text{secular}} = 45^\circ 28.5' + 5.46'T - 0.13'T^2, \quad (3)$$

S.D. = 11.6'

with       $T = t - 1966.0$ ,

where  $t$  is a calendar year. The values in 1976 are excluded in the least squares calculations, and the regression curves by eqs. (1)–(3) are given by each corresponding solid curve in Fig. 4, respectively. According to YOSHIMURA *et al.* (1977), the average secular changes during 1966–1973 were  $-131$  nT/year,  $-4.3'$  year $^{-1}$  and  $+3.3'$  year $^{-1}$ , respectively. The quadratic regression formulas by YOSHIMURA *et al.* (1977) have almost similar relations to eqs. (1)–(3), suggesting continuity of similar trends of secular variation to 1981 at Syowa Station. The first-order change  $-136$  nT/year in eq. (1) is consistent with the annual change in the vertical component (NAGATA, 1982). Since the secular change of total force is so large that, if the aeromagnetic surveys are made over a period of a few years, the obtained anomalies may be suspected to contain some ambiguity.

The synthetic secular variation at Syowa Station can be calculated by referring to the geomagnetic potential  $V(r, \theta, \lambda)$ , where

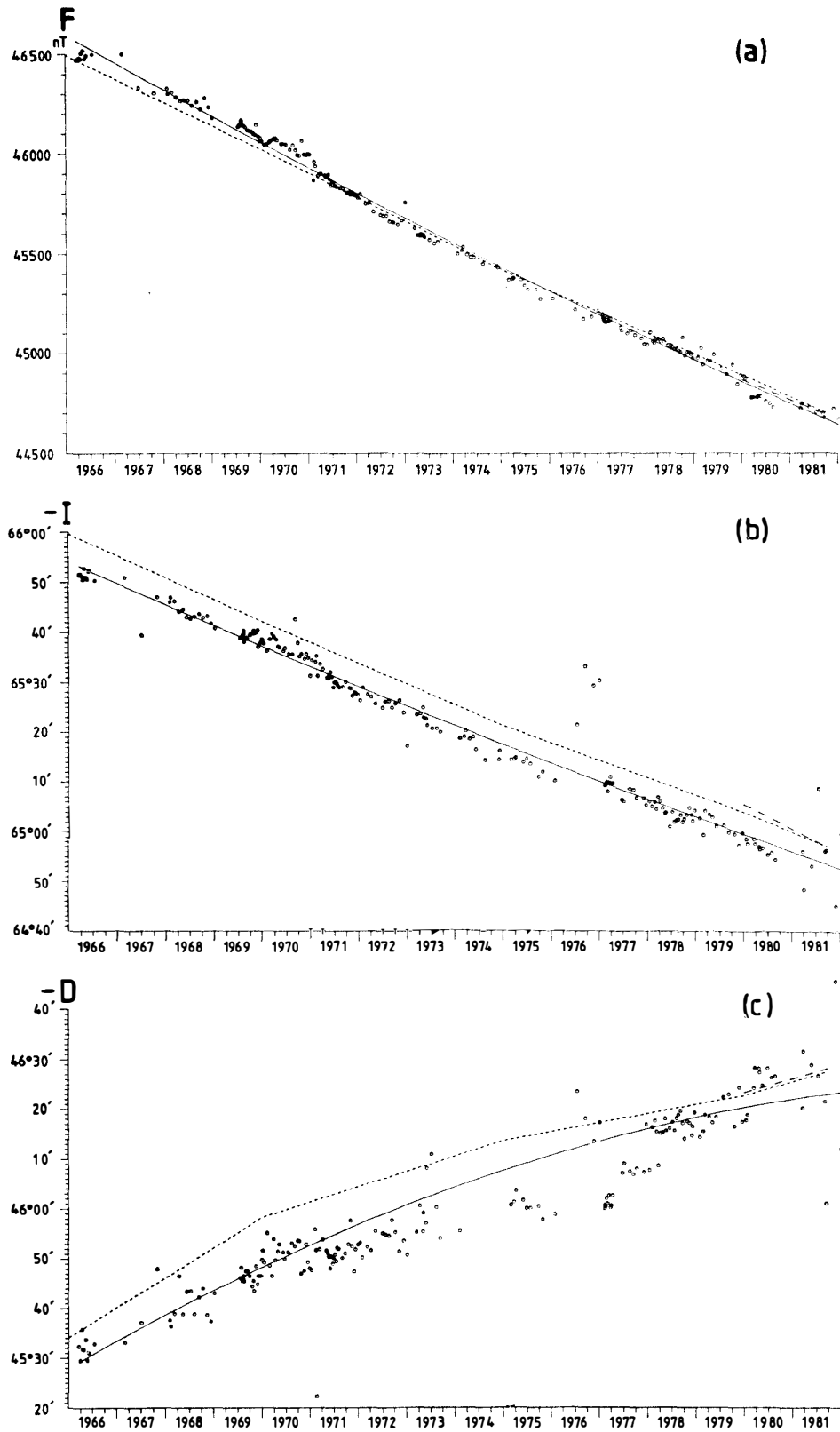


Fig. 4. Secular variations of geomagnetic total force  $F$  (Fig. 4a), inclination  $I$  (Fig. 4b) and declination  $D$  (Fig. 4c) at Syowa Station.

$$V = a \sum_{n=1}^{10} \sum_{m=0}^n \left( \frac{a}{r} \right)^{n+1} (g_n^m \cos m\lambda + h_n^m \sin m\lambda) P_n^m(\cos\theta). \quad (4)$$

Since the calculation of synthetic secular variation and IGRF in a region concerned is not our main purpose of this study and since their detailed derivations from eq. (4) are described in many textbooks on geomagnetism, the procedures and the notations in eq. (4) are not mentioned here. The spherical harmonic analysis with the Gauss' coefficients for IGRF 1965, IGRF 1970, IGRF 1975 and IGRF 1980, which were reported by IAGA Working Group I-1 (1981), results in the synthetic secular variation by thinner broken curves in Fig. 4. The difference between the synthetic and the least-squares regression secular variation at Syowa Station can be estimated from Fig. 4 and is about 30 nT for  $F$ , +5' for  $D$  and +6' for  $I$  in January 1981. The results of similar analysis for Magsat Field Model MGST (4/81), Epoch 1980 (NASA, MISSIONS UTILIZATION OFFICE, 1981) are also drawn in Fig. 4 by thicker broken curves for brief comparison during 1980–1981.

As for the regional distribution of the geomagnetic field, YOSHIMURA *et al.* (1977) had obtained an empirical quadratic function of latitude and longitude, based on 179 data along the oversnow traverse routes over the Mizuho Plateau. The isomagnetics had almost a parallel (northeast to southwest) direction with the gradient of approximately +8 nT/km toward the southeast direction in the areas of 68°–73°S in latitude and 34°–52°E in longitude. The regional change of the total force in 1981 around the Shirase Glacier, which can be synthesized from IGRF 1980, has almost the same patterns as those of Fig. 6 by YOSHIMURA *et al.* (1977) except the general decrease of 1200 nT by the secular variation during 1970–1981.

#### 4. Data Reduction to the Magnetic Anomaly

The acquired total force data on a digital cassette tape (Fig. 3) were edited on a 9-track open reel magnetic tape. The edited sequential data,  $F_{\text{observed}}$ , is a function of system clock time and can be distributed over each flight line as illustrated in Fig. 5-1a for the case of S1.  $F_{\text{observed}}$  is considered to include field of various origins, such as the geomagnetic reference field  $F_{\text{IGRF}}$ , diurnal variations by the earth's external field  $F_{\text{diurnal}}$ , magnetic anomalies by the local topographic and geological structures  $F_{\text{anomaly}}$ , and magnetic disturbance by the aircraft. When the sensing head was towed by a 10-m cable, magnetic disturbance by the small aircraft such as Cessna 185 or PC-6 was found negligible as mentioned by TAZIMA *et al.* (1972). The synthetic IGRF over S1 as a function of latitude, longitude and flight height can be arranged as a function of flight time (Fig. 5-1b), since the change rates of latitude and longitude can uniquely be determined at each sampling increment 1.2 s on the assumption of constant flight course and speed. The regional change of IGRF reaches 100 nT at both ends of S1. If the diurnal variations at Syowa Station can be considered as representing those over a 200 × 200 km extent, they can be treated as the reduction term for the survey over the Shirase Glacier. The three geomagnetic components at Syowa Station were digitally acquired on a 9-track open reel magnetic tape to the resolution of 0.1 nT and the sampling interval of 2 s. The synthesized total-force variations were converted

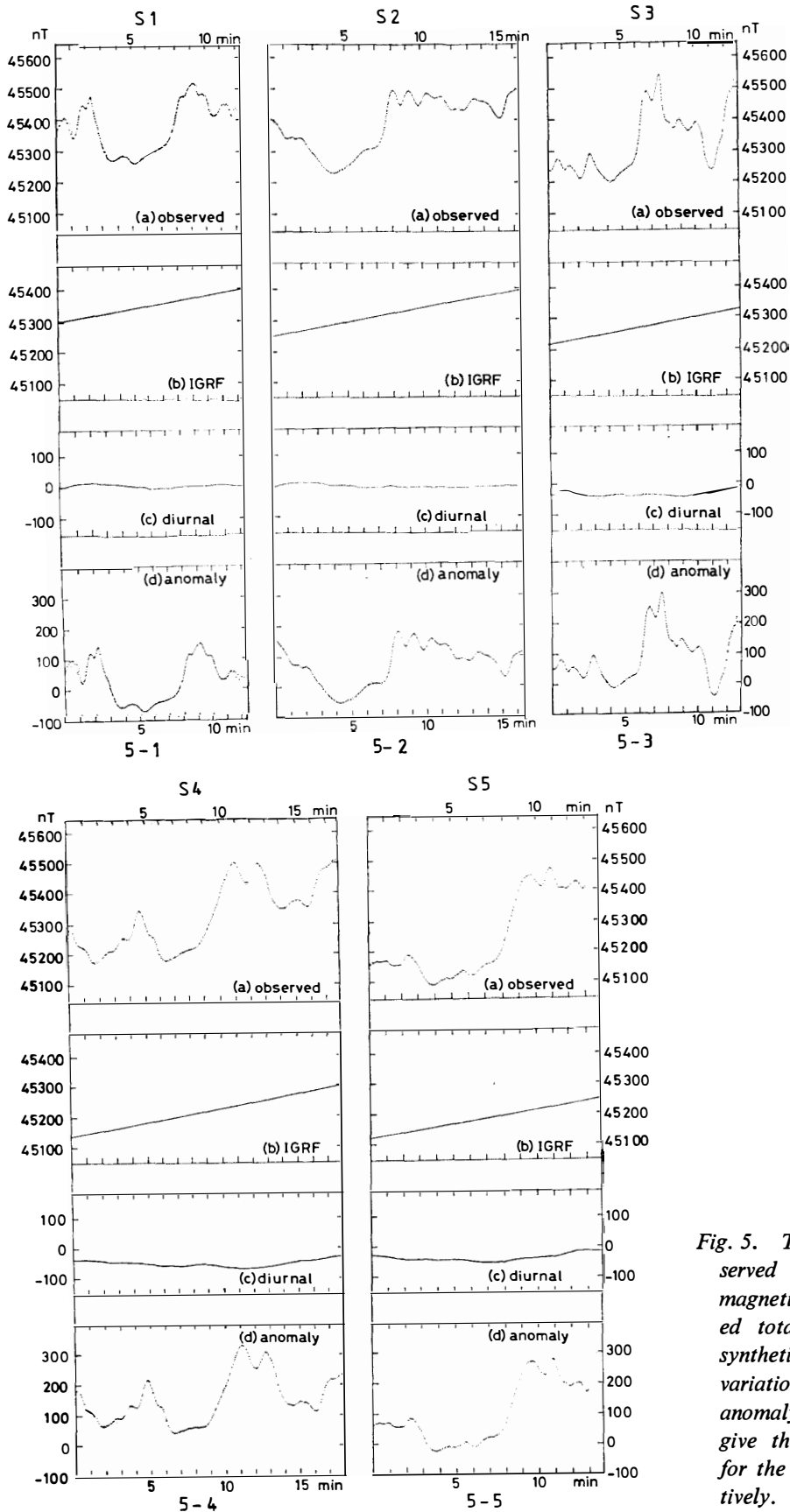


Fig. 5. The reduction of the observed total force data to the magnetic anomaly. (a) Observed total force variation, (b) synthetic IGRF, (c) diurnal variation, (d) reduced magnetic anomaly. Figures 5-1 to 5-5 give the reduction procedures for the profiles S1-S5, respectively.

into the time-series of 1.2 s interval (Fig. 5-1c) corresponding to the flight line over S1. The above three time-series,  $F_{\text{observed}}$ ,  $F_{\text{IGRF}}$  and  $F_{\text{diurnal}}$ , consist of equal data number and the subtraction of the second and the third time series from the first time-series gives  $F_{\text{anomaly}}$  (Fig. 5-1d) over S1. Similarly, Figs. 5-2 to 5-5 give the reduction procedures to the anomalies over S2 to S5, respectively. Figure 6 summarizes thus obtained anomaly profiles which are superposed onto the isomagnetic contours of IGRF for November 1980. They are considered to be caused mainly by the local topographic and geological structures of the Shirase Glacier.

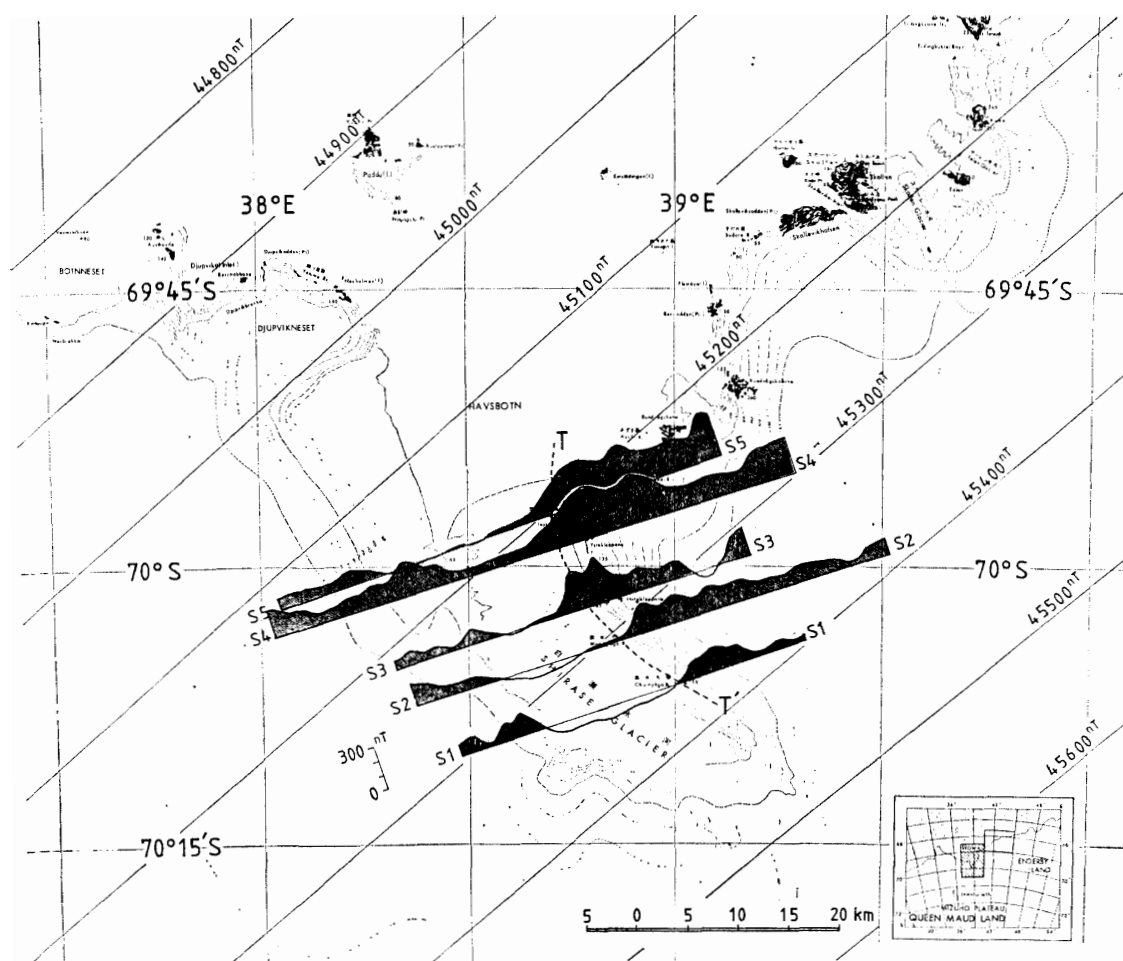


Fig. 6. Magnetic anomaly profiles over the Shirase Glacier which are superposed onto the isomagnetic contours of IGRF for November 1980.

The quantitative estimate of errors in the obtained anomalies is rather difficult. Since there were three clock systems in the survey, probable offsets 1–5 s among them result in the systematic error in the obtained anomalies. The estimate of errors becomes further vague by the uncertain fluctuation of flight speed and its course by the unknown factors of the wind speed and its direction. The maximum probable error, however, may come from the mismapping of the flight line and/or the anomaly profile

onto the topographic sheet, since the control point on each flight line is only one or two as illustrated in Fig. 2. A probable shift of  $60 \text{ m/point} \times 15\text{--}25 \text{ point} \sim 900\text{--}1500 \text{ m}$  has to be considered from a 20–30 s uncertainty of the pass time through each mark in the rock area.

### 5. Interpretation of the Magnetic Anomaly

The obtained anomaly profiles in Fig. 6 have systematic low values over the Shirase Glacier. There are two positive anomaly highs which reach 100–300 nT on both sides of the Shirase Glacier. The anomaly patterns are asymmetrical with comparatively smaller values on the western side than on the eastern side. As a first-order approximation, we are going to interpret the anomalies by two-dimensionally modeled mag-

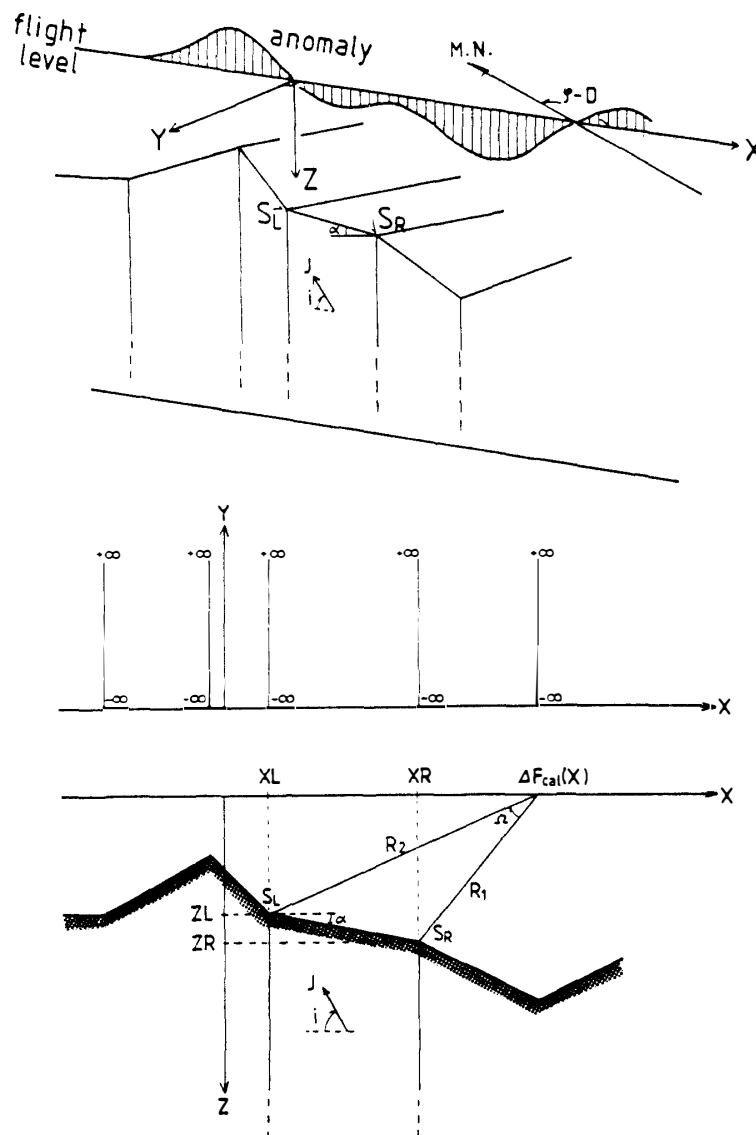


Fig. 7a. Schematic two-dimensional modeling of subglacial topography. The notations are summarized in Table 1.

netic bodies. Consider the Cartesian coordinates like Fig. 2, where  $X$  coincides with the flight direction,  $Y$  is perpendicular to  $X$  and  $Z$  is taken positive downward. Figure 7a gives schematic illustration of the model bodies, where each body is assumed as having a flat or inclined top surface which is extending infinitely in both positive and negative  $Y$  directions. The body is also assumed to extend infinitely in positive  $Z$  direction. The top surfaces of such bodies may be regarded as representing the model subglacial topography as shaded under broken lines in Fig. 7a. If homogeneous and uniform magnetization vector  $\mathbf{J}$  is assumed in the direction of the present earth's magnetic field, theoretical anomaly of each body can be expressed after JOHNSON (1969) as

$$\Delta F_{\text{cal}}(X) = F_x \cos i + \Delta F_z \sin i, \quad (5)$$

with

$$\Delta F_x = (R \cos \alpha - 2\Omega \sin \alpha)M - 2\Omega N, \quad (6-1)$$

$$\Delta F_z = (-R \sin \alpha - 2\Omega \cos \alpha)M - RN, \quad (6-2)$$

$$M = -|\mathbf{J}|(\sin i \cos \alpha + \cos i \sin \alpha), \quad (6-3)$$

$$N = |\mathbf{J}| \cos i, \quad (6-4)$$

$$R = \log(R_2/R_1)^2, \quad (6-5)$$

$$\Omega = \angle S_L X S_R, \quad (6-6)$$

$$i = \tan^{-1} \{ \sin I / \cos I \cos(\varphi - D) \}, \quad (6-7)$$

where the notations are summarized in Fig. 7a and Table 1. The synthetic anomaly by a series of two-dimensional body can be calculated by superposing each anomaly expressed by eq. (5). In the region concerned, the inclination  $I$  is  $65.3^\circ$  (upward). The projected dip angle  $i$  onto the  $XZ$  plane results in  $78.5^\circ$  from eq. (6-7), since the angle between the profile direction and magnetic north becomes  $116^\circ$ . The lower part of Fig. 7b illustrates the test topography with the normalized height of 2.5 and the

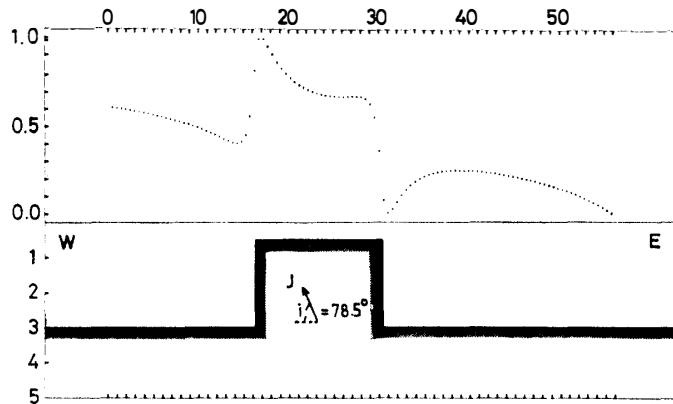


Fig. 7b. The lower part gives the test topography, where the normalized depth is measured from the flight level. The dotted curve in the upper part gives the normalized synthetic anomaly against the normalized horizontal distance.

normalized horizontal extent of 14. When the uniform magnetization of  $i=78.5^\circ$  is assumed under the whole shaded area, the normalized theoretical anomaly can be given by dotted curves as illustrated in the upper part of Fig. 7b. Though the calculated anomalies have an eastwardly declined linear trend, the correspondence of anomaly peaks with the topographic rise is rather good like that of the gravimetric case.

If there are  $p$  bodies,  $5p$  parameters have to be dealt in the calculation of synthetic anomaly profile, that is, four configuration parameters  $X_L$ ,  $X_R$ ,  $Z_L$ ,  $Z_R$  and magnetic susceptibility  $\kappa=|J|/F_0$  of each body by  $p$ . An interactive computer graphic display system was programmed by referring to OGAWA and TSU (1976), and the trial-and-error change of model topography was made by iteratively comparing the approximated synthetic anomaly curve with the observed anomaly curve. If  $p$  becomes larger, the matching of the above two curves may become better. However, a simpler modeling is desired since exact uniqueness cannot be assured in the trial and error procedures. Though the westwardly inclined magnetization emphasizes synthetic anomalies to the western side as illustrated in Fig. 7b, the observed anomalies have opposite sense of trends. Therefore, several trial and error modelings immediately reveal that constant

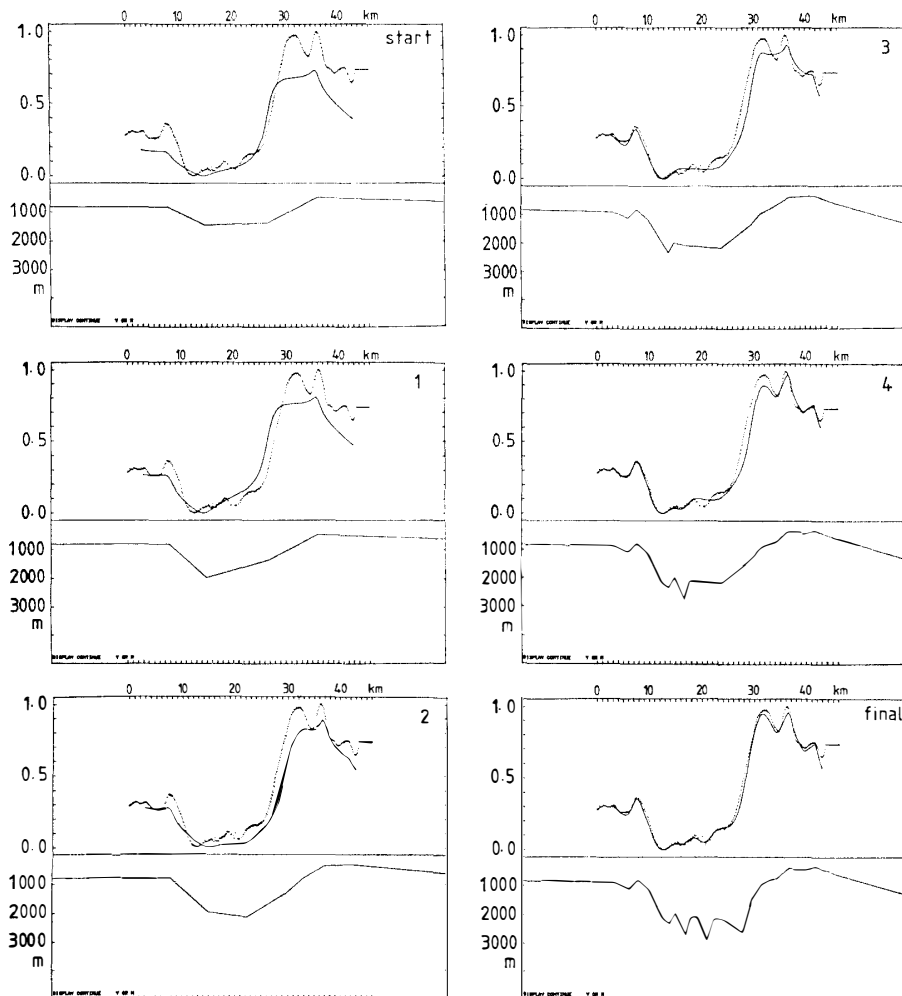


Fig. 8. An iterative approximation procedure of the synthetic anomaly to the observed anomaly by the computer graphic display for the profile S5.

and uniform magnetization results in the necessity of unsubstantial troughs with slopes of  $45^{\circ}$ – $60^{\circ}$  and 6000 m bottoms. It was then assumed that the eastern portion of model bodies has larger magnetic susceptibility  $\kappa_E$  than that of the western portion  $\kappa_W$ , and that their ratio is constant. It was further assumed that the transition took place around the eastern coast of the Shirase Glacier as schematically illustrated by broken curve T-T' in Fig. 6. Among the probable combination of  $\kappa_E$  and  $\kappa_W$  in the range of  $10^{-2}$ – $10^{-4}$  emu/cc, more than 20 case studies were made and a most probable combination of susceptibility  $\kappa_E = 2.4 \times 10^{-3}$  emu/cc (fixed) and  $\kappa_W = 1.5 - 1.8 \times 10^{-3}$  emu/cc was obtained. Figure 8 illustrates an iterative approximation procedure for the profile S5. The upper half of each figure gives the normalized observed anomaly (dotted curve) and the synthetic anomaly (solid curve), while the solid segments in the lower half give the model topography with the depth measured from the flight level (solid straight line). The change of topography was made under the constraints that the neighboring bodies did not have vertical gaps and the elevation of the rock area in Fig. 2 was in a reasonable range. In order to minimize the truncation error effect, matching of both extremities of the anomaly profile was not considered. The general amount of discrepancy, different trend of curvature, cross point between the two curves, etc. have to be considered in the approximation. By carefully increasing the number of bodies from a simpler topography, the matching of the two anomaly curves can be proceeded from the start model to the final model through 4 iteration stages as sum-

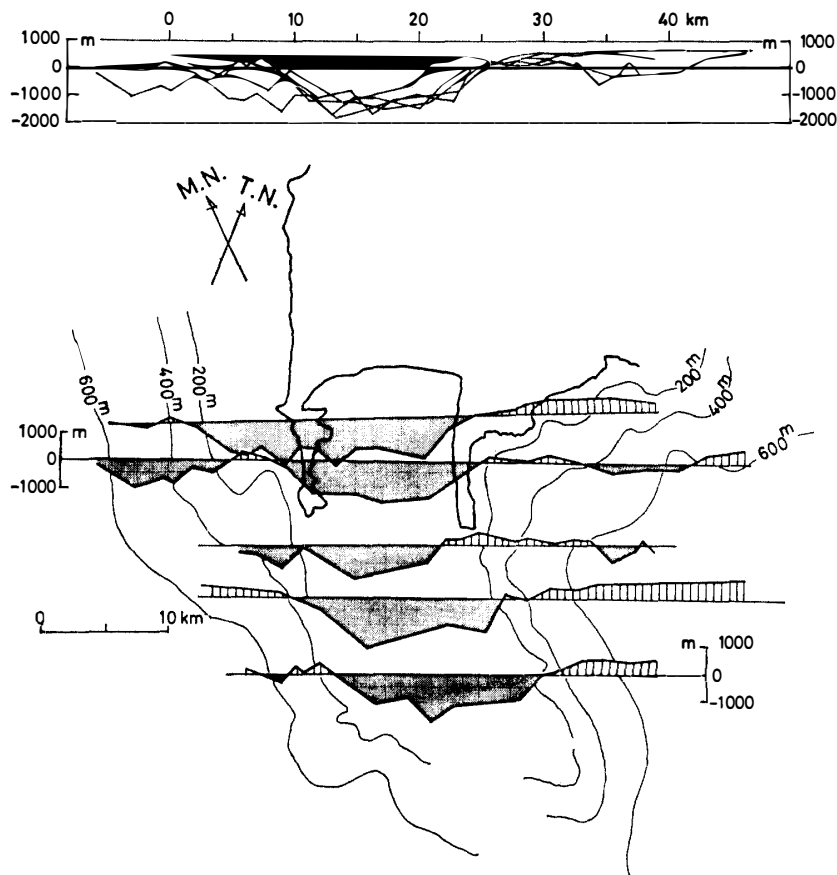


Fig. 9. The interpreted subglacial topography beneath the Shirase Glacier.

marized in Fig. 8. Likewise, two-dimensional modeling was proceeded for all of the anomaly profiles and they are summarized in the lower part of Fig. 9. The interpreted subglacial topography can be characterized by a north-south extending trough of 1800–2000 m depth and 15–20 km width. The trough corresponds remarkably well with the airphotographed flow region. As illustrated in the upper part of Fig. 9, the superposition of the five model topographic profiles, which are fitted to the broken curve T-T' in Fig. 6, gives moderate variation on the eastern coast and fluctuating variation on the western coast of the trough.

## 6. Discussion

The above modelings were proceeded under the simplification of the geological structures of the region concerned and its validity has to be examined. In 1980, JARE-21 made several explosion seismic experiments in the Ongul Islands and along the oversnow traverse route from Syowa to Mizuho Stations in the northern part of the Mizuho Plateau. According to IKAMI *et al.* (1982), the composite seismograms showed almost zero intercept time of 6.0 km/s travel time curve. The obtained velocity structures suggested a typical shield structure with negligibly thin sedimentary layers. The major geologic structures are considered as Precambrian shield. Geological studies also show no existence of sedimentary rocks or thick sedimentary deposits in and around Lützow-Holm Bay. The absence of sedimentary layers is advantageous for the simplification to the single and uniform magnetic layer beneath the ice layer. The assumption of infinite extent in  $Y$  direction under each profile does not hold exactly. However,  $\lambda_p/d \geq 1$  holds for most part of the profiles, where  $\lambda_p$  denotes the half wave-length between neighboring flight lines and  $d$  does the depth to the bedrock. The obtained each anomaly profile can thus be considered as mainly determined by the general trend of topography under each flight line.

An airborne radio-echo sounding was for the first time made by JARE-20 over the Shirase Glacier. According to WADA and MAE (1981), the obtained bedrock topography showed about 250 m below sea level at point B (70°20'S, 39°20'E) approximately 30 km upstream from S1, and showed a moderate increase or undulation of bedrock relief for further upstream direction. However, the reflected echo from the bedrock was masked by the ghosts caused by crevasses and cracks in ice mass and the bedrock topography which corresponds to profiles S1–S5 could not efficiently be obtained. As for the downstream region, the sea bottom topography of Lützow-Holm Bay has recently been extensively studied by the echo sounder, *e.g.* MORIWAKI (1979) and MORIWAKI and YOSHIDA (1983). The cross sections along the east-west direction (see Fig. 4 by MORIWAKI and YOSHIDA, 1983) clearly indicate the existence of a north-south extending trough from 1600 m depth (at 69°52'S) to 1200 m depth (at 69°40'S) with the horizontal width of 15–20 km. The trends of bedrock topography by radio-echo sounding, by aeromagnetic survey and by echo sounder along the flow lines of the Shirase Glacier from upstream to downstream are consistent with one another and agree well with the formation of drowned glacial trough by the expansion of the ice sheet.

On the eastern coast of the Shirase Glacier, there are several rock areas exposed

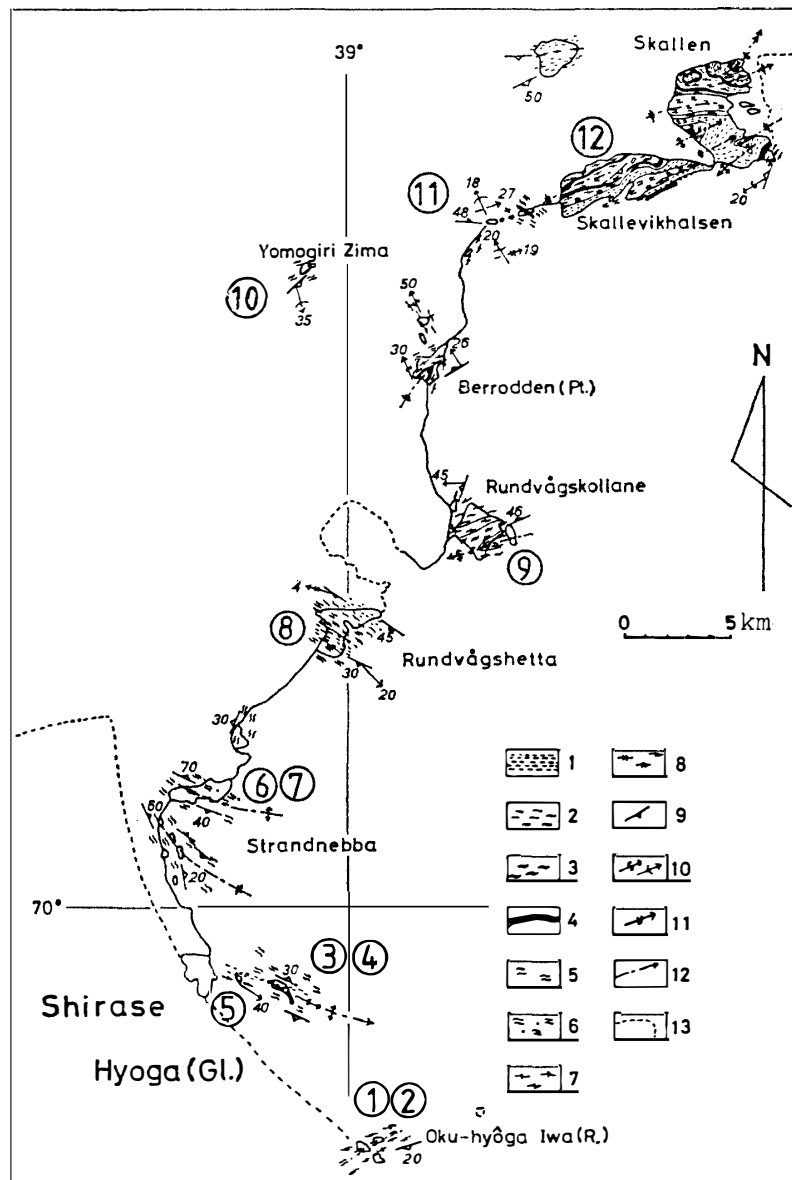


Fig. 10. Geologic sketch of the southern region of the Sôya Coast, reproduced from YOSHIDA (1978) with the author's courtesy. 1: Siliceous gneiss with intercalations of basic gneiss. 2: Biotite gneiss. 3: Metabasites. 4: Marble bed. 5 and 6: Charnockitic rocks. 7: Garnet-bearing gneissose granite. 8: Pink gneissose granite. 9: S-plane. 10: Microfold lineation. 11: Crenulation lineation. 12: Folding axis. 13: Fringe of ice shelf or glacier. The circled number indicates the sample number in the measurement of magnetic susceptibility.

from the ice sheet. Figure 10 illustrates the geological sketch of the southern part of the Sôya Coast which is redrawn from YOSHIDA (1978). Susceptibility data of the sample rocks from these areas were measured and they are summarized in Table 2. Though the two samples from Oku-hyôga Rock, which is located at the southernmost coast of the Shirase Glacier, have rather large values in the order of  $10^{-3}$  emu/cc, most of the data are in the order of  $10^{-5}$ – $10^{-4}$  emu/cc. Since the obtained anomalies were in the order of  $10^2$  nT, average susceptibility in the order of  $10^{-3}$  emu/cc was inevitably

Table 2. Ground data on magnetic susceptibility.

Sample No.	Area	Rock No.	Rock	Density (g/cc)	Susceptibility (emu/cc)
1	Oku-hyôga Rock	A69100602*	Pink gneissose granite	2.57	$1.21 \times 10^{-3}$
2	"	A69100606*	Metabasite in the charnockitic rock	2.87	$3.06 \times 10^{-3}$
3	Instekleppane	A69100805*	Gneissose-biotite granite	2.69	$0.849 \times 10^{-3}$
4	"	A69100804*	Orthopyroxene-biotite-pl rock (metabasite)	2.94	$34.8 \times 10^{-6}$
5	Azarashi Rock	A69100810*	Charnockitic gneiss	2.60	$0.714 \times 10^{-3}$
6	Strandnebbba	A69100811*	"	2.59	$0.103 \times 10^{-3}$
7	"	Unnamed	"	2.61	$0.440 \times 10^{-3}$
8	Rundvågshetta	Y69101005*	Siliceous gneiss	2.62	$1.59 \times 10^{-6}$
9	Rundvågskollane	Y69100705*	Charnockitic gneiss	2.71	$13.3 \times 10^{-6}$
10	Yomogiri Island	Y69100804*	Sillimanite-garnet quartzofeldspathic gneiss	2.56	$7.30 \times 10^{-3}$
11	Sudare Rock	A69101101*	Clinopyroxene-phlogopite marble	2.62	$0.726 \times 10^{-3}$
12	Skallevikhalsen	Unnamed	Gneissose biotite granite	2.60	$5.12 \times 10^{-6}$

\* After YOSHIDA and ANDO (1971).

necessary on the assumption of homogeneous and uniform magnetization in the direction of the present earth's magnetic field. The introduction of the geomagnetic boundary (T-T' in Fig. 6) was rather arbitrary for the sake of modeling and it was not based on the geologic background. Since the systematic sea-bottom topographic discontinuity of 200–300 m level on both sides of the Shirase Glacier suggests a large geological discontinuity as indicated by MORIWAKI and YOSHIDA (1983), systematic analyses of geomagnetic and petrological characteristics are required on both sides of the Shirase Glacier.

#### Acknowledgments

This research is a passing consideration before the completion of geomagnetic anomaly map over the Mizuho Plateau. However, the two-dimensional consideration may be a useful step to the three-dimensional consideration on geophysically almost unknown areas of Antarctica. The authors are indebted to H. TSU and T. NAKATSUKA of the Geological Survey Institute for their suggestions and encouragements. Dr. M. YOSHIDA kindly gave us rock samples and determined the rock type described in column 4 of Table 2. Dr. M. FUNAKI let us use the Bison magnetic susceptibility meter. Discussions with K. MORIWAKI and K. SHIRAISHI of the National Institute of Polar Research were very helpful. In order to obtain the aeromagnetic data, one of the authors (K. SHIBUYA) was always supported by all the members of JARE-21 led by Dr. S. KAWAGUCHI. He expresses his special thanks to T. MIZUSHIMA, T. YASHIRO, H. OOMORI, Y. KATSUTA and T. TAKAGI in the operations by PC-6. This research was partly financed by the budget for JARE, entitled "Geophysical investigation of the crust and upper-mantle structure around Syowa Station, East Antarctica (representative: T. NAGATA)". Calculations were made by HITAC M160II at the National Institute of Polar Research.

## References

- BEHRENDT, J. C., DREWRY, D. J., JANKOWSKI, E. and GRIM, M. S. (1982): Results from an aeromagnetic and radio echo ice-sounding survey over the Dufek intrusion, Antarctica. Fourth International Symposium on Antarctic Earth Sciences, August 1982, Volume of Abstracts, comp. and ed. by P. R. JAMES *et al.* Adelaide, Univ. Adelaide, 13.
- IKAMI, A., ITO, K., SHIBUYA, K. and KAMINUMA, K. (1982): Crustal structure of the Mizuho Plateau, Antarctica, revealed by explosion seismic experiments. Fourth International Symposium on Antarctic Earth Sciences, August 1982, Volume of Abstracts, comp. and ed. by P. R. JAMES *et al.* Adelaide, Univ. Adelaide, 87.
- IAGA WORKING GROUP I-1 (1981): International Geomagnetic Reference Field, 1980, in short articles, notices and useful information. IAGA News, 20, 100–102.
- JOHNSON, W. W. (1969): A least-squares method of interpreting magnetic anomalies caused by two-dimensional structures. Geophysics, 34, 65–74.
- KANEKO, H. (1976): Purinsu Orafu Kaigan chiiki no kôkû jiki sokuryô (Aeromagnetic survey in the vicinity of Prince Olav Coast, Antarctica). Nankyoku Shiryô (Antarct. Rec.), 55, 61–68.
- MORIWAKI, K. (1979): Submarine topography of the central part of Lützow-Holm Bay and around Ongul Islands, Antarctica. Mem. Natl Inst. Polar Res., Spec. Issue, 14, 194–209.
- MORIWAKI, K. and YOSHIDA, Y. (1983): Submarine topography of Lützow-Holm Bay, Antarctica. Mem. Natl Inst. Polar Res., Spec. Issue, 28, 247–258.
- NAGATA, T. (1982): Geomagnetic secular variation in the Antarctic region during 1960–1975. Nankyoku Shiryô (Antarct. Rec.), 74, 27–44.
- NASA, MISSIONS UTILIZATION OFFICE (1981): Magsat Information Bulletin, 6, 5p.
- OGAWA, K. and TSU, H. (1976): Magnetic interpretation using interactive computer graphics. Jpn. Pet. Dev. Corp. Rep., 3, 126p.
- RENNER, R. G. B., DIKSTRA, B. J. and MARTIN, J. L. (1982): Aeromagnetic surveys over the Antarctic Peninsula. Antarctic Geoscience, ed. by C. CRADDOCK. Madison, Univ. Wisconsin Press, 363–370.
- TAZIMA, M., KAKINUMA, S., YOSHIDA, M., MASUDA, M. and YOSHIMURA, A. (1972): Ryutsuo-Horumu Wan to sono engan chiiki no kôkû jiki sokuryô (Aeromagnetic survey in the vicinity of Lützow-Holm Bay, Antarctica). Nankyoku Shiryô (Antarct. Rec.), 44, 69–78.
- WADA, M. and MAE, S. (1981): Airborne radio echo sounding on the Shirase Glacier and its drainage basin, East Antarctica. Nankyoku Shiryô (Antarct. Rec.), 72, 16–25.
- YOSHIDA, M. (1978): Tectonics and petrology of charnockites around Lützow-Holmbukta, East Antarctica. J. Geosci., Osaka City Univ., 21, 65–152.
- YOSHIDA, M. and ANDO, H. (1971): Geological surveys in the vicinity of Lützow-Holm Bay and the Yamato Mountains, East Antarctica. Report No. 1 of the geology section of the 10th Japanese Antarctic Research Expedition. Nankyoku Shiryô (Antarct. Rec.), 39, 46–54.
- YOSHIMURA, A., ABE, Y. and NARUSE, R. (1977): Distribution of three geomagnetic components over Mizuho Plateau, Antarctica. Nankyoku Shiryô (Antarct. Rec.), 60, 38–46.

(Received April 4, 1983; Revised manuscript received May 23, 1983)